COMPUTATIONAL OPTIMIZATION OF A STOCHASTIC MODEL FOR SIMULATING APOPTOTIC SIGNALINGT

OPTIMIZACIÓN COMPUTACIONAL DE UN MODELO ESTOCÁSTICO PARA LA SIMULACIÓN DE LA SEÑALIZACIÓN APOPTÓTICA

J. German-Serra[a†], N. López-Marín[a]

Faculty of Physics, University of Havana, La Habana, Cuba; jorge.german@fisica.uh.cu[†]
† corresponding author

Recibido 30/1/2025; Aceptado 30/6/2025

The development of mathematical models to simulate biological processes is essential for understanding the complexity of living systems, allowing for predictions and virtual experiments that would be difficult to carry out under real conditions. In this work, we present a mathematical model to simulate the process of apoptosis or programmed cell death, using the Gillespie algorithm. Additionally, an optimization of this model is proposed, which reduces computation time and enables the model to simulate apoptosis in the cells of a tumor under topical treatment. Results are also presented demonstrating that both models are equivalent. The optimization reduced the execution time of the simulation by two days.

El desarrollo de modelos matemáticos para simular procesos biológicos es fundamental para comprender la complejidad de los sistemas vivos, permitiendo hacer predicciones y realizar experimentos virtuales que serían difíciles de llevar a cabo en condiciones reales. En el presente trabajo presentamos un modelo matemático para simular el proceso de apoptosis o muerte programada en una célula, utilizando el algoritmo de Gillespie. Se propone además, una optimización de este modelo, que permite disminuir el tiempo de cálculo y utilizar el modelo para simular la apoptosis en las células de un tejido tumoral que fue sometido a un tratamiento tópico. Se presentan además resultados que demuestran que ambos modelos son equivalentes. La optimización permitió disminuir el tiempo de ejecución de la simulación en dos días.

Keywords: Stochastic models (modelos estocásticos); Complex systems (sistemas complejos); Computer modeling (modelado computacional); Monte Carlo methods (métodos de Monte Carlo); Systems biology (biología de sistemas).

I. INTRODUCTION

Apoptosis, or programmed cell death, is a vital biological process that facilitates the controlled elimination of unnecessary or damaged cells. This mechanism plays a crucial role in maintaining a stable internal environment, even in the face of external changes, and ensures the proper functioning of the tissues. Dysregulation of apoptosis is associated with various diseases, particularly neurodegenerative disorders and cancer. In cancer, malignant cells often develop the ability to evade apoptosis, allowing them to survive and proliferate uncontrollably. Understanding the complex mechanisms that govern apoptosis and its disruptions is essential to develop targeted therapies. These therapies aim to reactivate apoptotic pathways, promoting the selective death of cancer cells while minimizing damage to normal tissues, ultimately enhancing the efficacy of treatment and improving patient outcomes [1–7].

Given the high costs associated with developing less invasive and more effective treatments, mathematical modeling of apoptosis presents a promising tool to increase our understanding of this cellular process. Specifically, computational algorithms that efficiently simulate all biochemical interactions within cells can provide valuable insights into the behavior of cancer and other diseases. Using these models, researchers can better predict outcomes and tailor therapies to individual patient needs. Various mathematical models used to simulate apoptosis are based on different approaches, including agent-based models [8–10], Boolean networks [11, 12] , differential equations [14–16], and stochastic methods grounded in Monte Carlo simulations using their own algorithms or the Gillespie algorithm [17–19].

In the study of physical systems where randomness is fundamental, traditional deterministic methods often prove insufficient. In these cases, the Gillespie algorithm, originally developed to model stochastic chemical reactions, becomes highly relevant in physics. This algorithm enables accurate simulation of discrete, random processes over time, including phenomena such as particle diffusion [20] , molecular population dynamics [21], and the evolution of non-equilibrium systems. Its versatility makes it a powerful tool in fields like statistical physics, biophysics, and materials science, especially when microscopic fluctuations have significant macroscopic consequences.

In this work, we present a mathematical model of cell death by apoptosis that incorporates the internal dynamics of biochemical species within the cell. In addition, we introduce an optimized version of the model, demonstrating results that validate its accuracy and equivalence. We apply this enhanced model to simulate apoptosis in cells of an epithelial tumor undergoing topical treatment and present the results of these simulations.

II. METHODS

II.1. Apoptosis model

The activation of the intrinsic pathway of apoptosis illustrated in Figure 1. This process begins with the permeabilization of the mitochondria, which leads to the release of cytochrome C (CytC) into the cytoplasm. The regulation of mitochondrial membrane permeabilization involves the Bcl-2 protein family, which can promote or inhibit apoptosis by directly influencing channels in the outer mitochondrial membrane. Specifically, Bax facilitates the formation of pores, while Bcl-2 acts to inhibit it. Once cytochrome C is released into the cytoplasm, it triggers the assembly of a multiprotein complex known as the apoptosome, which subsequently activates the caspase cascade via caspase-9 (C9), resulting in cell death by apoptosis. Additionally, after membrane permeabilization, the SMAC protein (Second Mitochondria-derived Activator of Caspases) is released into the cytoplasm, where it binds to inhibitors of apoptosis (XIAPs). This binding prevents XIAPs from stopping the apoptotic process, allowing apoptosis to progress [22].

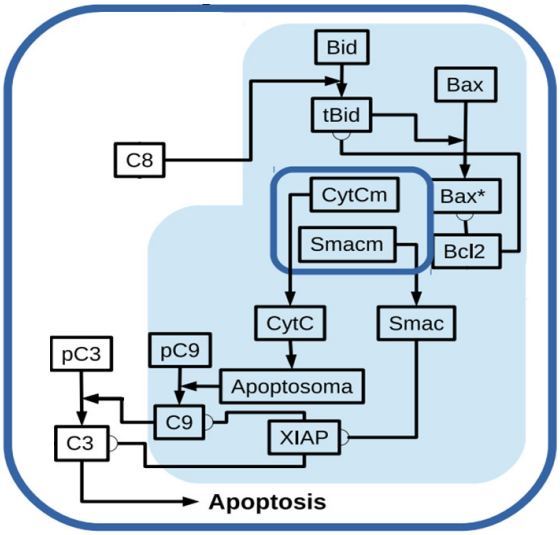

Figure 1. Intrinsic pathway of apoptosis activation. Cell degradation by apoptosis begins when Caspase 3 (C3) is activated. The intrinsic pathway is shaded in blue and begins when pores open in the mitochondrial membrane, and Cytochrome C (CytC) and SMASCs are released into the cytosol. Cytochrome C forms a protein complex, Apoptosome, which activates C3 through C9. The Bcl-2 protein family regulates the formation of pores in the mitochondrial membrane: Bax and/or Bak, represented by Bax in the model, are responsible for the formation of the pores, while Bcl-2, Bcl-xL, or Mcl-1, represented by Bcl-2, inhibit it.

The Gillespie algorithm was used to simulate cell death by apoptosis. This is a stochastic simulation method designed to model the time evolution of chemical reactions in systems with a finite number of molecules. The algorithm captures the inherent randomness of the reaction events by simulating the waiting times between reactions and determining which reaction occurs next on the basis of their rates. It operates under the Markovian assumption, meaning that the future state of the system depends only on its current state. Using exponential distributions to model waiting times and random sampling to select reactions, the Gillespie algorithm effectively simulates complex biochemical processes [23,24].

Table 1. Reactions that participate in the intrinsic pathway

No	Reaction
1	C8 + Bid → C8:Bid
2	C9 + Bid → C9:Bid
3	Bid + Bax → Bid:Bax
4	Bid:Bax → tBid + Bax
5	tBid + Bax → tBid:Bax
6	tBid:Bax → tBid + Bax
7	Bid2 + Bax → Bid2:Bax
8	Bid2:Bax → Bid2 + Bax
9	Cytc + Apaf → Apop
10	Apop + pC9 → Apoptosome:2pC9
11	Apoptosome:2pC9 → Apop + 2pC9
12	C9 + C9 → C9:C9
13	C9:C9 → C9 + C9
14	XIAP + Smac → XIAP:Smac
15	XIAP:Smac + pC9 → XIAP:pC9
16	XIAP:pC9 → XIAP + pC9
17	Apaf + Apaf → Apaf:Apaf
18	Apaf:Apaf → Apaf + Apaf
19	Cytc + CytC → Cytc:CytC
20	Smac → Smac

The interactions within the intrinsic pathway of apoptosis, as depicted in Figure 1, are represented through the reactions listed in Table 1 and the corresponding molecules in Table 2. The rate constants for these reactions (K) were obtained from the literature [25,26]. These reactions take place inside the cell, specifically in the cytoplasm, which is assigned a volume of $\Omega = 1000\mu m^3$, reflecting the typical cytoplasmic volume. The model assumes that a healthy cell maintains an equilibrium among the concentrations of molecules such as Bid, Bax, Bcl-2, and the complexes Bcl2:tBid and Bcl2:Bax. Under these conditions, the levels of tBid and activated Bax are sufficiently low to prevent apoptosis. However, if this equilibrium is disrupted, the concentration of tBid rises, leading to cell death. To simulate this scenario, the initial concentration of tBid is set to a value greater than zero, and this value is proportional to the apoptotic signal. The model also considers that when the concentration of activated Bax reaches the threshold value of $10nM$, pores are formed in the mitochondrial membrane, activating reactions 19 and 20 from Table 1. Finally, the cell is considered dead when the Caspase-3 concentration reaches $10nM$.

All simulations were developed in the C programming language[1] and executed on a personal Asus computer equipped with an Intel® Celeron® CPU N3050, running at 1.60 GHz, with 4 GB of RAM and a 64-bit operating system.

II.2. Optimization of the apoptosis model

The simulation of apoptosis in a single cell takes approximately 7 seconds on the computer used for these calculations. To simulate apoptosis in a tissue composed of

[1] Although not publicly archived, the simulation code supporting this study will be made available to researchers upon formal request to the corresponding author

millions of cells, it is crucial to minimize this time as much as possible. This can be achieved either by using a more powerful computer or by optimizing the model for greater efficiency.

Table 2. Molecules and initial concentrations used in the model of cell death by apoptosis using the Gillespie algorithm.

Symbol	Description	$\mathbf{X}_0$ (nM)
$C8$	Active form of Caspase-8	0
Bid	BH3-binding domain death agonist	25
$C8 : Bid$	Complex of C8 with Bid	0
$C9 : Bid$	Complex of C9 with Bid	0
$pC3$	Procaspase-3, inactive	100
$C8 : p3$	Complex of Caspase-8 with procaspase-3	0
$C3$	Active form of Caspase-3	0
$C9 : pC3$	Complex of C9 with procaspase-3	0
$Apaf$	Activating Factor (Apaf-1)	80
$pC9$	Inactive form of Apoptosome-9	20
$Apop$	Apoptosome complex	0
$Apoptosome : 2pC9$	Complex of Apoptosome with 2 procaspase-9	0
$C9 : C9$	Complex of C9 with C9	0
$XIAP : Smac$	X-linked Inhibitor of Apoptosis	30
$XIAP : pC9$	Complex of XIAP with procaspase-9	0
$XIAP : C9$	Complex of XIAP with caspase-9	0
$Apaf : Apaf$	Complex of Apaf-1 dimer	0
$Cytc : CytC$	Cytochrome c inside the mitochondria	50
$Smac$	SMAC inside the mitochondria	50

The reactions that lead to the permeabilization of the mithochondrial membrane are more time consuming in the simulation. For this reason, we propose to eliminate the reactions [3–7] shown in Table 1 and replace them with a single reaction. This new reaction has tBid and Bax as reactants, tBid and activated Bax as products, and K as the rate constant of the optimized reaction (Figure 2). The new rate constant was chosen so that the time to permeabilize the membrane would be the same for both models. We used the original apoptosis model to determine the opening times of the mitochondrial membrane (t_{org}). Subsequently, using the optimized model, we change the parameter K to obtain the opening time of the membrane (t_i) for each value of K. Finally, we selected $K = K_i$ that corresponded to the t_i closest to t_{org}.

The strength of the apoptotic signal is directly proportional to the initial concentration of tBid, as previously discussed. In contrast, the initial concentration of Bcl2 influences membrane permeabilization but is not included in the reaction of the optimized model. To address this limitation, we calculated the values of K for various initial concentrations of these molecules, denoted as $[tBid_0]$ and $[Bcl2_0]$. This dependence requires the application of the previously described method each time these initial concentrations change, which is inefficient given our goal of applying this optimized model to a heterogeneous epithelial cell tumor, where cells exhibit varying initial concentrations of all molecules.

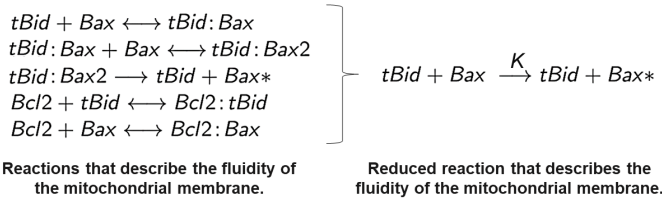

Figure 2. Reactions that permeabilize the mitochondrial membrane (left) and the resulting reaction in the optimized model (right).

To improve efficiency, we develop a matrix of K values for every combination of $[tBid_0]$ and $[Bcl2_0]$. We defined a range for initial tBid concentrations from $25nM$ to $2510nM$ with increments of approximately $38nM$, and for initial Bcl2 concentrations from $40nM$ to $60nM$ with increments of $5nM$. Consequently, we calculated the values of K for each combination, which resulted in a matrix with 67 rows and 21 columns. This matrix can be used in simulations involving multiple cells with different initial concentrations of the aforementioned molecules.

II.3. Simulation of apoptosis in an epithelial tumor

Using the optimized model of apoptosis, we successfully simulated an epithelial tumor after topical treatment. The tumor is modeled as a three-dimensional matrix of **m** layers deep and in each layer **n × n** cells. In this case, we modeled 6 layers of 100×100 cells each.

This model operates under the assumption that drug concentration decreases exponentially with increasing tumor depth. Since the initial concentration of tBid is directly related to the apoptotic signal, we modeled a tumor with a depth of $1mm$, where the initial concentration of tBid ($[tBid_0]$) decreases exponentially with depth. To incorporate cellular variability, we assumed that the initial levels of the relevant proteins differ between individual cells. The initial concentrations of these proteins were uniformly distributed around their mean values (see Table 2), with a variance of 20 %.

These simulations were performed on an Intel i7 computer with 12 cores and 16GB of RAM.

III. RESULTS AND DISCUSSION

III.1. Optimization of mithochondrial membrane permeabilization reactions

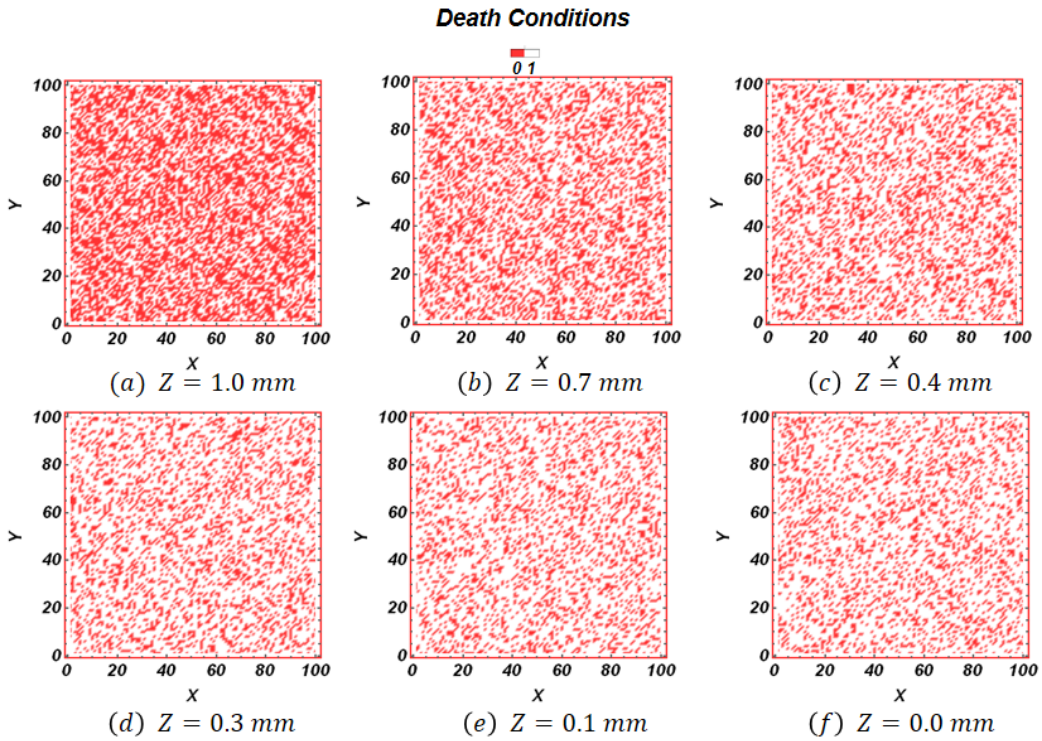

Figure 3. Cell survival matrices at different tumor depths after topical treatment of an epithelial tumor. The tumor is modeled as a three-dimensional matrix consisting of six layers, each containing 100×100 cells. Cell death by apoptosis was simulated: cells that died within 3500 seconds after treatment are shown in red, while surviving cells are shown in white.

In the apoptosis model, the mitochondrial membrane becomes permeabilized, leading to the release of CytC and SMASCs into the cytosol when the concentration of activated Bax reaches $10nM$, approximately 12040 molecules. To validate the functionality of the optimized model, we compare the time at which activated Bax reaches this threshold. Figure 4 shows only the first 200 seconds of the simulation in which the membrane opening occurred to demonstrate that in both models the time at which activated Bax reaches the membrane opening threshold concentration is quite similar, indicating that the two models are equivalent and confirming the precision of the determined value of K.

In the apoptosis model, mitochondrial membrane permeabilization occurs when activated Bax concentration reaches 10 nM (~ 12040 molecules), triggering the release of cytochrome c (CytC) and SMASCs into the cytosol. To validate the optimized model's functionality, we compared the time at which activated Bax reaches this threshold. Figure 4 displays the initial $200s$ of the simulations, demonstrating comparable threshold attainment times in both models. This kinetic equivalence confirms the consistency of the model and validates the determined parameter K.

III.2. Influence of Initial Concentrations of Bcl-2 and tBid on the Kinetic Constant of the reaction

We calculated K values for various initial concentrations of tBid and Bcl-2. Figure 5 presents the density plot of the resulting matrix. In particular, when the initial concentration of tBid exceeds $137nM$, K becomes independent of the initial concentration of Bcl-2.

We initially performed a tumor simulation on a small scale. In this model, the tumor is represented as a three-dimensional array consisting of 67 layers, each layer corresponding to a specific value of $[tBid_0]$ in the K matrix calculated previously. Within each layer, we simulate cell death by apoptosis for 100 cells arranged in a 10 x 10 grid.

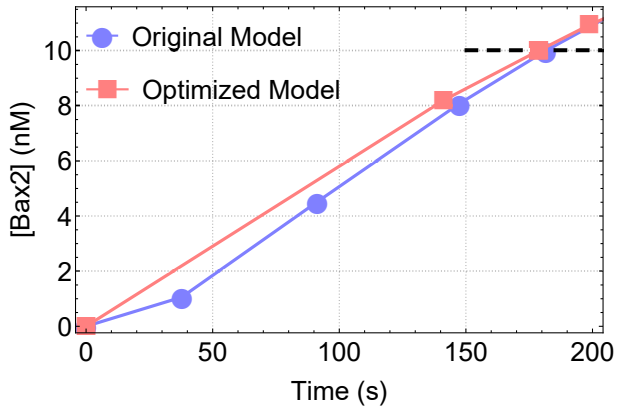

Figure 4. Activated Bax concentration as a function of time for both models. The black dashed line at 10 nM indicates that the times of mitochondrial membrane permeabilization are similar.

The initial concentrations of the other proteins involved in the apoptosis process varied around the mean values presented in Table 2. For the simulation, we assumed that if a cell did not undergo apoptosis within 3500 seconds, which is the mean time of cell death by apoptosis, it would continue to survive.

This approach allowed us to calculate the number of dead cells in each layer, as illustrated in Figure 6.

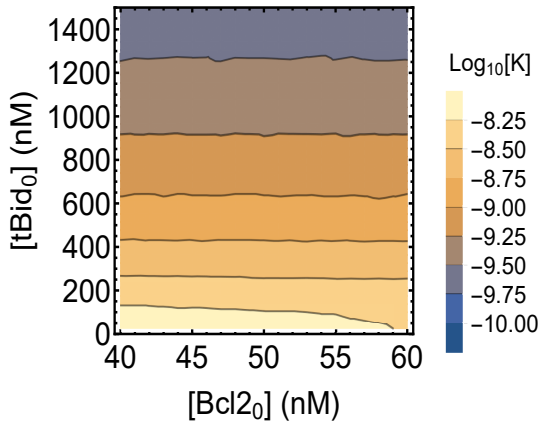

Figure 5. Density plot of the kinetic constant K as a function of the initial concentrations of tBid and Bcl-2 in logarithmic scale.

In particular, in the upper layers of the tumor (where $[tBid_0] > 251nm$, corresponding to $Z < 0.5\ mm$), the number of dead cells does not increase as $[tBid_0]$ increases. This result can be explained by considering that, when the initial concentration of tBid is very high, the likelihood of the optimized reaction occurring is also significantly elevated in the Gillespie algorithm. Consequently, until Bax is fully consumed, none of the other reactions in the model that contribute to increasing Caspase-3 levels and subsequent cell death takes place (see Table 2, references [26–29],).

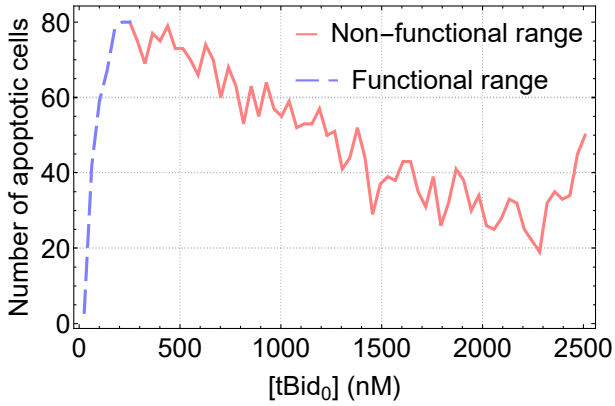

Figure 6. Number of dead cells as a function of tBid initial concentration. In blue, the functional range in which $[tBid_0]$ is proportional to the apoptotic signal.

To maintain the initial concentration of tBid proportional to the strength of the apoptotic signal, we selected initial concentrations in the range of 61 to $251nM$ for our subsequent simulations. By narrowing the range of $[tBid_0]$ values, we refined the K matrix used in the model, as shown in Figure 7. This adjustment highlights that at low concentrations of tBid, variations in Bcl-2 become increasingly influential. This effect is attributed to the distinct propermeabilizing and antipermeabilizing functions that each protein performs, respectively.

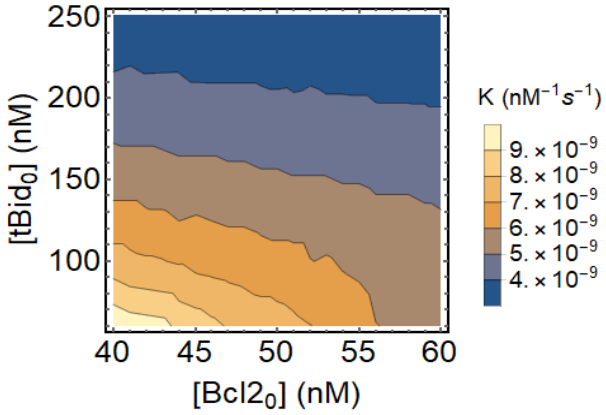

Figure 7. Density plot of the kinetic constant K as a function of the initial concentrations of tBid and Bcl-2.

III.3. Simulation of cell death by apoptosis in tumor tissue

Using the results of the previous section, we simulated an epithelial tumor treated with a topical drug to investigate how the number of cells undergoing apoptosis changes as a function of depth and the initial concentration of tBid. The tumor is modeled as a three-dimensional matrix consisting of six layers, each containing a 100 x 100 grid of cells. We assume that the average initial concentration of tBid in each of the six layers decreases exponentially. This approach is supported by experimental evidence that shows that topical drug application enhances absorption in the upper layers of the skin [30,31].

In the simulations, a cell was considered to undergo apoptosis if death occurred before 3500 seconds. In this case, it was assigned a value of 1. In contrast, if the cell did not die, it was assigned a value of 0. The density plots representing the matrices at various values of Z are presented in Figure 3. Dead cells are white and those that survive are red. It can be seen that as the depth increases, the density of cells that undergo apoptosis decreases. This result is in agreement with experimental data that demonstrate that some topical treatments are effective only for superficial tumors [32].

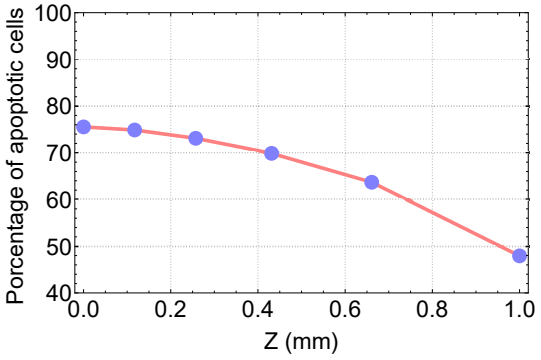

Figure 8. Percentage of dead cells versus tumor depth (Z). The tumor is modeled as a three-dimensional matrix consisting of six layers, each with 100×100 cells. A cell was considered apoptotic if it died within 3,500 seconds of treatment. For each layer, the percentage of dead cells was calculated.

To get an idea of the exact number of cells that died as a function of Z, we show these results in Figure 8. Almost 75 % of

the cells near the surface died from apoptosis and this number decreases as the depth of the tumor increases. At 1 *mm* depth, more than 50 % cells survive.

III.4. Simulation time versus optimization

Figure 9 compares the simulation times for both models in simulations with different initial concentrations of Bcl-2, while keeping the initial concentrations of other molecules constant.

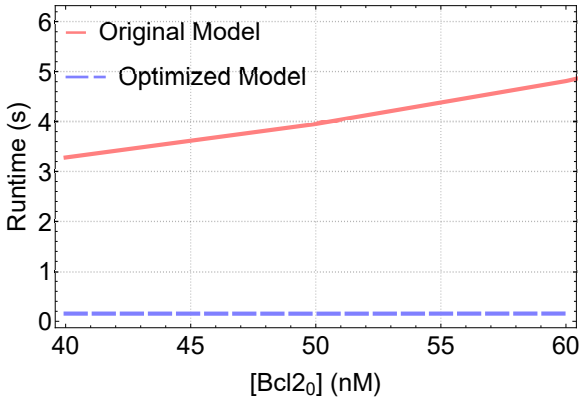

Figure 9. Simulation time as a function of the initial concentration of Bcl-2 for the apoptosis model that includes all reactions of membrane permeabilization (original) and the one that includes only one reaction (optimized).

The recorded time reflects how long each simulation takes to complete the membrane permeabilization process, which involves the set of simplified reactions. This time represents how long both simulations take to complete the permeabilization process of the membrane, where the set of reactions that we simplify participate. We can see that by increasing the initial concentration of Bcl-2, keeping $[tBid_0]$ constant, the time of the original model increases, while in the optimized model it is practically independent of this variable. In particular, at high initial concentrations of Bcl-2, the advantages of our optimization become even more pronounced. Given that this model will be applied to thousands of cells within tumor tissue, optimization is significantly improved.

In Tables 3 and 4 we show a comparison of simulation times for various initial concentrations of tBid and Bcl-2. The concentration values in the tables were selected as the limits used in our tumor simulations.

Table 3. Simulation time for the unoptimized model (s)

Concentration	**tBid$_0$ = 62.7 nM**	**tBid$_0$ = 250.8 nM**
Bcl2o = 40nM	3.90	3.515
Bcl2o = 60nM	6.626	4.406

Table 4. Simulation time for the optimized model (s)

Concentration	**tBid$_0$ = 62.7 nM**	**tBid$_0$ = 250.8 nM**
Bcl2o = 40nM	0.24861	0.134928
Bcl2o = 60nM	0.341222	0.144051

These results demonstrate that the performance of the optimized model is superior. To help the reader better understand the machine time saved with the proposed optimization, we present a straightforward calculation. We simulate 10000 cells across 6 layers. If each cell requires 6.626*s* to open the membrane, representing the maximum possible time, the total computational time would be $6 \times 10000 \times 6.626 = 397560$ s, which is equivalent to approximately 4.5 days of simulation. In contrast, using the optimized model, the maximum simulation time would be $6 \times 10000 \times 0.341 = 20460$ s, or about 5.6 hours. This significant reduction in machine time demonstrates that our optimization represents a significant advance in the study of cell death by apoptosis.

IV. CONCLUSION

In this study, we have developed a model that qualitatively simulates cell death by apoptosis, capturing the timing and concentration dynamics of key molecules involved in the intrinsic pathways. Our optimization of the equations governing mitochondrial membrane permeabilization has significantly reduced simulation times without compromising the accuracy of the cell death timing or the qualitative behavior of the involved molecules. The findings regarding the independence of K from Bcl-2 concentrations at high tBid levels provide valuable insights into the complex interactions within apoptotic signaling pathways. The substantial reduction in computation time enhances the feasibility of applying our model to simulate apoptosis in tissues containing large numbers of cells, making it a powerful tool for studying cell death in various biological contexts, particularly in tumor environments. Our model not only contributes to a deeper understanding of apoptosis but also lays the groundwork for future research aimed at exploring therapeutic strategies that target apoptotic pathways. We believe that this work will facilitate further advancements in computational biology and cancer research, ultimately leading to improved treatment approaches for diseases characterized by dysregulated apoptosis.

V. ACKNOWLEDGEMENTS

REFERENCES

[1] S. Kumari, R. Dhapola, D. H. Reddy, Apoptosis **28**, 943 (2023).

[2] V. K. Sharma, T. G. Singh, S. Singh, N. Garg, S. Dhiman, Neurochem. Res. **46**, 3103 (2021).

[3] C. Hu, X. Zhang, N. Zhang, W.-Y. Wei, L.-L. Li, Z.-G. Ma, Q.-Z. Tang, Clin. Transl. Med. **10**, e124 (2020).

[4] K. Tsuchiya, Microbiol. Immunol. **64**, 252 (2020).

[5] B. A. Carneiro, W. S. El-Deiry, Nat. Rev. Clin. Oncol. **17**, 395 (2020).

[6] O. Morana, W. Wood, C. D. Gregory, Int. J. Mol. Sci. **23**, 1328 (2022).

[7] M. Jiang, L. Qi, L. Li, Y. Li, Cell Death Discov. **6**, 112 (2020).

[8] B. Roche, J. M. Drake, P. Rohani, BMC Bioinform. **12**, 1 (2011).

[9] B. N. Brown, I. M. Price, F. R. Toapanta, D. R. DeAlmeida, C. A. Wiley, T. M. Ross, T. D. Oury, Y. Vodovotz, Math. Biosci. **231**, 186 (2011).
[10] J. S. Yu y N. Bagheri, Front. Bioeng. Biotechnol. **8**, 249 (2020).
[11] H. Sizek, A. Hamel, D. Deritei, S. Campbell, E. Ravasz Regan, PLoS Comput. Biol. **15**, e1006402 (2019).
[12] P. Dutta, L. Ma, Y. Ali, P. Sloot, y J. Zheng, BMC Syst. Biol. **13**, 1 (2019).
[13] L. C. Gomes-Pereira, M. Chaves, J. Roux, en *2020 28th Mediterranean Conference on Control and Automation (MED)* (IEEE, 2020), pp. 887–892.
[14] P. Schröder, A. Wagner, D. Stöhr, M. Rehm, y W. Ehlers, PAMM **19**, e201900310 (2019).
[15] M. Hendrata, J. Sudiono, Comput. Math. Methods Med. **2016**, 1 (2016).
[16] R. M. Schmitz, S. M. Willerth, G. van Rensburg, R. Edwards, J. Med. Biol. Eng. **40**, 41 (2020).
[17] R. A. Gatenby, Y. Artzy-Randrup, T. Epstein, D. R. Reed, y J. S. Brown, Cancer Res. **80**, 613 (2020).
[18] P. P. González-Pérez, M. Cárdenas-García, en *International Conference on Practical Applications of Computational Biology & Bioinformatics* (Springer, 2018), pp. 17–26.
[19] J. H. Buchbinder, D. Pischel, K. Sundmacher, R. J. Flassig, I. N. Lavrik, PLoS Comput. Biol. **14**, e1006368 (2018).
[20] D. Bernstein, Phys. Rev. E **71**, 041103 (2005).
[21] A. M. Kierzek, Bioinformatics **18**, 470 (2002).
[22] R. Abbas, S. Larisch, Cells **9**, 663 (2020).
[23] D. T. Gillespie, J. Phys. Chem. **81**, 2340 (1977).
[24] D. T. Gillespie, Annu. Rev. Phys. Chem. **58**, 35 (2007).
[25] S. Raychaudhuri, E. Willgohs, T.-N. Nguyen, E. M. Khan, T. Goldkorn, Biophys. J. **95**, 3559 (2008).
[26] J. G. Albeck, J. M. Burke, S. L. Spencer, D. A. Lauffenburger, P. K. Sorger, PLoS Biol. **6**, e299 (2008).
[27] F. Fantini, A. Greco, C. Del Giovane, A. Cesinaro, M. Venturini, C. Zane, T. Surrenti, K. Peris, P. Calzavara-Pinton, J. Eur. Acad. Dermatol. Venereol. **25**, 896 (2011).
[28] M. Rehm, H. J. Huber, H. Dussmann, J. H. Prehn, EMBO J. **25**, 4338 (2006).
[29] N. J. Waterhouse, J. C. Goldstein, O. Von Ahsen, M. Schuler, D. D. Newmeyer, D. R. Green, J. Cell Biol. **153**, 319 (2001).
[30] B. Newell, W. Zhan, J. Control. Release **360**, 447 (2023).
[31] J. J. Calcutt, M. S. Roberts, Y. G. Anissimov, Pharm. Res. **39**, 783 (2022).
[32] N. Gupta, G. Gupta, D. Singh, Front. Nanotechnol. **4**, 1006628 (2022).